Coherent Raman spectroscopy of the quantum-entangled exciton-Mn^{2+} state in CdTe

D. Wolverson, L. C. Smith, S. J. Bingham, and J. J. Davies
Department of Physics, University of Bath, Bath BA2 7AY, United Kingdom
(Received 3 August 2012; published 15 October 2012)

Electron paramagnetic resonance of Mn^{2+} ions in CdTe was detected using coherent Raman electron spin resonance spectroscopy (CRESR) with microwave frequencies of 13.8 and 33.7 GHz. It was possible to resolve the effects of both the hyperfine interaction between the Mn^{2+} $3d^5$ electrons and the manganese nucleus and the cubic crystal field. From the optical resonance profile, it is shown that the coherent Raman signal is resonant with an excitonic state and is due to the exchange interactions between the Mn^{2+} $3d^5$ electrons and the hole of the exciton. The existence of a CRESR signal under these circumstances provides a direct demonstration that coherence is maintained between the exciton and Mn^{2+} systems via this exchange interaction.

DOI: 10.1103/PhysRevB.86.155209 PACS number(s): 78.30.Hv, 75.50.Pp, 76.30.−v, 71.35.−y

I. INTRODUCTION

The Mn^{2+} ion is well known as a substitutional impurity having high solubility in II-VI, III-V, and IV-VI semiconductors; it generally forms a paramagnetic center with electronic configuration $3d^5$ and a spin angular momentum $S = 5/2$. The resulting giant effective g factors of the band carriers in bulk samples and in dilute magnetic semiconductor (DMS) quantum wells have been very well studied.[1] Recent work has focused on, for instance, the exploitation of the high degree of spin-polarization of mobile carrier gases in DMS quantum wells,[2,3] the possibility of obtaining ferromagnetism in DMS materials,[1,4] the behavior of van Vleck ions [e.g., Fe in CdTe (Ref. 5)] and the exploration of alloys or heterostructures in which the effects of different magnetic species are combined. In addition, it has recently proved possible to observe the ultimate nanoscale limiting case of the interaction of a single Mn^{2+} ion with the confined states of a single quantum dot.[6] The coherent interaction of a single donor-bound exciton with several Mn^{2+} ions in a quantum well, on the other hand, is very interesting in the context of quantum computing as an example of an optically induced quantum entangled state,[7] which is amenable to control via ultrafast pumping.[8]

Coherent Raman electron spin resonance (CRESR) spectroscopy is a promising technique for the investigation of the electronic properties of DMS quantum structures.[9,10] The CRESR method (discussed in the next section) retains the sensitivity and optical selectivity of conventional spin-flip Raman scattering (SFRS)[11] but, being based on electron spin resonance (ESR),[12] its energy resolution is no longer limited by a diffraction grating-based spectrometer or by the laser linewidth. The application of optically detected magnetic resonance (ODMR) to the study of DMS materials is not new; ODMR was instrumental in identifying the exchange interaction between magnetic ions and excitons in some of the earliest work (for example, Ref. 13). Recently, various forms of ODMR have been applied to DMS bulk crystals and quantum wells.[14–18]

A key distinction between CRESR and other forms of ODMR lies in the fact that, in CRESR, optical and microwave fields develop a finite degree of coherence when spin and optical resonance conditions are simultaneously met; this allows the use of sensitive heterodyne detection of the optical signal. The requirement of optical resonance conditions means that CRESR offers a site-selective ESR probe which depends on both ground and excited optical states and which has a wide range of potential applications; for example, the CRESR technique has been applied to the nitrogen-vacancy (NV) complex in diamond,[19] another system of great interest in optical quantum information processing applications[20] and to studies of metal centers in metalloproteins.[21–23] In semiconductors, SFRS has proved useful to probe the spin-dependent excitations of free carrier gases[2,3] and of carriers localized at impurities;[24,25] for the latter application, we demonstrated the dramatically improved resolution of CRESR compared to SFRS and also gave an analysis of its sensitivity.[26] As we show, a special feature of CRESR in DMS systems is the simultaneous coherent excitation of the exciton and manganese spin states (in contrast to the other material systems just mentioned, for which optical excitation takes place directly into the localized electronic states of the paramagnetic center).

However, in the original demonstration of CRESR of the localized $3d^5$ electrons of Mn^{2+}[9] it was not possible to resolve *directly* the Mn^{2+} fine and hyperfine structure, though its existence was inferred from the overall line shape and width. Furthermore, the optical resonance behavior and its relationship to the excitonic states of the semiconductor were not analyzed. Here, we develop a proper treatment of the excitonic intermediate states and show that a detailed simulation of the observed spectra is then possible.

II. EXPERIMENTAL DETAILS

Details of our experimental CRESR system have been given elsewhere[9,26] and analogous techniques have been applied much earlier to nuclear magnetic resonance.[27,28] The technique can be visualized using a three-level Λ-type energy diagram, shown on the right in Fig. 1. A microwave magnetic field of angular frequency ω is applied to the sample together with a slowly swept orthogonal magnetic field **B**. When the energy difference between levels $|1\rangle$ and $|2\rangle$ is brought into coincidence with $\hbar\omega$, spin resonance is achieved, inducing a finite degree of coherence between these levels.[29]

The excitation photon energy is tuned to match the energy difference between levels $|1\rangle$ and $|3\rangle$, inducing a coherence between these two levels. Consequently, there is some degree of coherence between levels $|2\rangle$ and $|3\rangle$. Thus, at spin resonance,

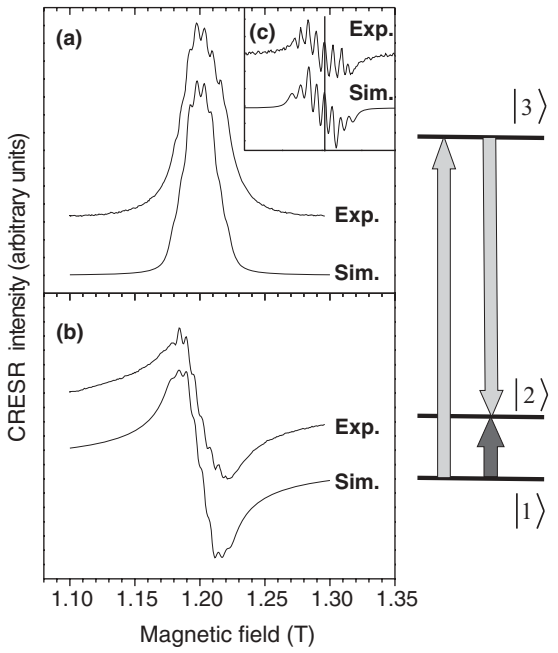

FIG. 1. Experimental and simulated coherent Raman-detected ESR (CRESR) signal of Mn^{2+} in CdTe with a microwave frequency of 33.7 GHz and laser energy of 1.601 eV: (a) absorptive component; (b) dispersive component; (c) numerical derivatives of the experimental and simulated absorptive components. (Right panel) Schematic diagram of the three-level system involved in the CRESR process; light arrows represent optical transitions at resonance and the dark arrow represents the microwave transition at resonance.

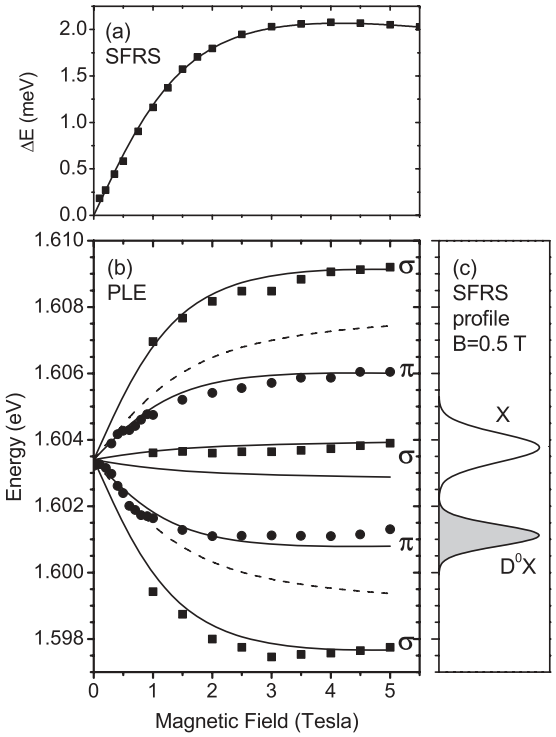

FIG. 2. Magnetic field dependence in the Voigt geometry (light propagating normal to the applied magnetic field) of (a) conduction band electron SFRS shifts in the bulk (Cd,Mn)Te sample and (b) its PLE spectra (points are experimental data and solid lines are simulations; dashed lines show the predicted energies of optically forbidden transitions). (c) The strength of the electron SFRS signal at 0.5 T as a function of excitation energy (lines are fits to experimental data and the two curves are normalized to the same peak height).

the emitted coherent Raman wave and the laser excitation beam develop a degree of both spatial and temporal coherence and so copropagate. They are brought to beat with one another in a fast photodiode and the resulting microwave signal from the photodiode is detected by mixing it with a signal from the microwave oscillator that provides the microwave field at the sample. Similar to ESR, a quadrature mixer provides both absorptionlike and dispersionlike signals,[27,28] as shown in Figs. 1(a) and 1(b), respectively. To ensure that the Raman-scattered and excitation beams are not orthogonally polarized, circularly polarized excitation is used (modulated between left and right circular states) allowing lock-in detection of the signals at the outputs of the microwave mixer. The resulting resolution and sensitivity limits were analyzed earlier.[26]

Here, a dilute (Cd,Mn)Te crystal was used to study the CRESR of Mn^{2+} ions in CdTe (Mn concentration ~0.5%). The sample was first characterized using SFRS of the conduction band electrons and photoluminescence excitation (PLE) spectroscopy (Fig. 2) and conventional ODMR.[9,10,16] From fitting the dependence of the electron SFRS on a magnetic field with the Brillouin function appropriate for $J = 5/2$ (Ref. 11), taking into account also the band structure g-factor contribution of $g = -1.67 \pm 0.01$ [which we obtain from our own and other SFRS measurements on CdTe (Ref. 30)], we determined the effective paramagnetic Mn concentration to be $\bar{x} = 0.0048 \pm 0.0001$ [see Fig. 2(a)]; we take the values of the $s - d$ and $p - d$ exchange parameters $N_0\alpha$ and $N_0\beta$ to be 0.22 and −0.88 eV, respectively.[31] The PLE data [Fig. 2(b), points] gave the energies of the free exciton states as a function of magnetic field, in good agreement with energies calculated using the value of $\bar{x}$ derived from the SFRS data [Fig. 2(b), lines]. This crystal was also studied previously using CRESR with a 13.8-GHz microwave source[9] and here we have extended that work to 33.7 GHz.

III. Mn^{2+} COHERENT RAMAN SIGNAL

Figures 1(a) and 1(b) show that the CRESR signals of Mn^{2+} in this sample consist of several finely spaced components. To emphasize this structure, we show in Fig. 1(c) the numerical derivative of the absorptive component. Simulations of the experimental data are also shown; these take account of the hyperfine coupling between the Mn $3d^5$ electrons and the ^{55}Mn nucleus (spin $I = 5/2$, 100% abundance) and of the effect of the cubic crystal field on the $3d$ state. These can be described for a single Mn^{2+} ion by the following spin Hamiltonian with magnetic field $\mathbf{B}$ directed along the crystallographic z axis[12,32]:

$$H = g_{\mathrm{Mn}}\mu_B \mathbf{S}\cdot\mathbf{B} + A\mathbf{I}\cdot\mathbf{S} + a\left(S_x^4 + S_y^4 + S_z^4 - \tfrac{3}{5}S^4\right). \quad (1)$$

The hyperfine interaction gives six equally spaced lines which are then each split into a further five components by the crystal field. In agreement with earlier work, we take $|A| = 5.9$ mT and the cubic field coefficient $|a| = 3$ mT.[9,14,32] The signal of

Fig. 1 is centered at a magnetic field of 1.201 T, consistent with the g factor of the Mn $3d^5$ electrons of $g = 2.00$.

IV. ROLE OF INTERMEDIATE EXCITONIC STATES

From our earlier study of the CRESR of donors in ZnSe (Ref. 26), we anticipate that the resonant intermediate states of CRESR are the same as those of (incoherent) SFRS and are excitonic and, thus, are properties of the semiconductor band structure rather than of the paramagnetic center itself. This is in contrast to all previous CRESR experiments such as, for example, Cr^{3+} in ruby, where the optical resonance was directly with *internal* transitions of the Cr^{3+} ions[33] or the nitrogen-vacancy complexes in diamond[19] where, again, localized excitations of the scattering center provided the intermediate state.

In order to understand better the coherent Raman mechanism in this case, we consider first the resonance behavior of incoherent SFRS in our bulk (Cd,Mn)Te sample. The intensity of the SFRS of conduction band electrons was measured as a function of excitation energy at $B = 0.5$ T (this field was chosen to be close to the spin resonance field for Mn with $g = 2$- and 13.8-GHz microwave excitation). Gaussian fits to the data are shown in Fig. 2(c) and show two bands. The first, labeled X, is centered on the free (or weakly localized) exciton energy levels at 1.6038 eV and coincides with the zero-field PLE maximum. At this low magnetic field, resonances within this band due to the different exciton Zeeman components are not resolved. A second band at a lower energy of 1.6011 eV is also detected; this is attributed, as in the case of ZnSe (Ref. 26), to a resonance with an exciton bound to a neutral donor (D^0X); its shift of 2.7 meV below the X resonance is consistent with the localization energy of excitons at shallow donors in CdTe of about 3 meV (Ref. 34). The ground state of the donor-bound exciton complex is the paramagnetic neutral donor (D^0) and it is the unpaired electron of this center that gives rise to the SFRS signal of Fig. 2(a).

Turning to the CRESR data, the spectra of Fig. 1 were obtained with a laser energy of 1.601 eV. By comparison with Fig. 2, it is not possible from this data alone to say whether the resonant intermediate state is the free exciton, X, or the donor-bound exciton, D^0X, since the Zeeman components of these two types of exciton overlap significantly at a magnetic field of 1.2 T and both have optical transitions in the region of 1.601 eV. The D^0X components, not shown in Fig. 2 since they were not detected in PLE, consist of an identical manifold to those of X shown in Fig. 2 but displaced downwards in energy by the localization energy of 2.7 meV. We return to the question of the intermediate excitonic state in Sec. V.

A feature of the present problem is that the coupling between the optical and the spin states involved in CRESR is fundamentally different to the cases of Cr^{3+} in ruby, the NV center in diamond, or D^0X in ZnSe. Here, the intermediate excited state $|3\rangle$ consists of an exciton (X or D^0X[30]); it is coupled to the Mn d electrons which undergo the spin flip process only via the s-d or p-d exchange interactions of its electron and hole respectively. One model was developed earlier[35,36] to explain the observation of Mn SFRS in (Cd,Mn)Te in terms of a "flip-flop" process in which, via these exchange interactions, there is a change in exciton spin state together with an opposite change in the spin state of a single Mn ion. This is consistent with, first, the observed resonance energies and, second, the observed polarization selection rules for SFRS, namely, that Mn SFRS is allowed in a backscattering geometry for processes $\bar{z}(\sigma\pi)z$ and $\bar{z}(\pi\sigma)z$ in conventional notation, where the light propagation direction $\bar{z}$ is perpendicular to the applied magnetic field.

However, one can question whether this model is adequate when the intermediate excitonic state couples to a larger number N of Mn ions, as in our case [we estimate $N \sim 29$ (Ref. 16)]. The problem of the ESR and SFRS of a donor-bound electron interacting with several Mn ions has already been analyzed[37] and it is shown there that, in fact, the exchange-coupled spins of the localized carrier and the Mn ions should be treated as a single, collective spin state; for small N, this model leads to a complicated ESR or SFRS line shape. Nevertheless, it is predicted that, for large N, the SFRS spectrum converges to one similar to that of an isolated Mn^{2+} ion[37] for which the flip-flop model can be applied. Since the present sample with $x \sim 0.0048$ is in the limit of large N, we are justified in using the simple spin Hamiltonian of Sec. III.

V. MODEL

A quantitative model for coherent Raman processes involving three-level systems based on the density matrix formalism was developed initially to describe nuclear magnetic resonance[27,28] and was extended later to the case of transition metal ions such as Cr^{3+} in ruby.[29] We apply here only the expressions derived in Ref. 29 for the CRESR line shape appropriate for our particular experimental setup (in the terms of Ref. 29, where a full derivation may be found, this is viewed as a form of circularly polarized magnetic circular dichroism experiment as first discussed in Ref. 38). The basic double Lorentzian line shape which expresses both the optical and the microwave resonances is given in Ref. 29 by Eq. (2):

$$\Lambda_{123}(\omega_L,\omega_{MW}) = \frac{1}{\omega_{23}-\omega_L-\omega_{MW}+i\gamma_{23}} \times \left[\frac{\rho_{33}^{(0)}-\rho_{11}^{(0)}}{\omega_{13}-\omega_L+i\gamma_{13}}+\frac{\rho_{22}^{(0)}-\rho_{11}^{(0)}}{\omega_{21}-\omega_{MW}+i\gamma_{21}}\right], \quad (2)$$

in which terms of form ω_{xy} represent the transition energies (divided by $\hbar$) between states x and y and γ_{xy} represents their linewidths. The laser and microwave angular frequencies are ω_L and ω_{MW}, respectively, and the steady-state populations of states x are represented by ρ_{xx}^0. The contribution S to the total signal which arises from a particular set of levels $|1\rangle,\ldots,|3\rangle$ that is obtained with the polarization modulation scheme we employed was shown (Ref. 29) to be based on this fundamental line shape as follows:

$$S \propto (\mu_{13}^{-*}\mu_{23}^{-}-\mu_{13}^{+*}\mu_{23}^{+}) \times \Lambda_{123}^{*}(\omega_L,\omega_{MW}) - (\mu_{13}^{-}\mu_{23}^{-*}-\mu_{13}^{+}\mu_{23}^{+*}) \times \Lambda_{123}(\omega_L,-\omega_{MW}), \quad (3)$$

where μ_{ij} is the matrix element for the transition between states i and j and $+,-$ denote the two circular polarization states. These matrix elements are, in the present case, those between the zinc-blende valence and conduction bands for the

Voigt geometry [that is, for the light propagation direction perpendicular to the applied slowly varying magnetic field, so that σ and π transitions (indicated in Fig. 2) are both possible via electric dipole transitions, and correspond to linear polarizations normal and parallel, respectively, to the magnetic field].

In order to obtain the total signal at any particular magnetic field and excitation energy, it is then necessary to sum S of Eq. (3) over *all* three-level Λ-type diagrams arising from the four valence band ($J = 3/2$) and two conduction band ($S = 1/2$) spin states. This summation allows the possibility of interference between signals arising from different three-level systems which, as has been noted before, can lead even to complete cancellation of some signals.[39,40] It should be noted that this summation requires that the matrix elements for σ and π transitions referred to above are calculated taking into account their relative complex phases as well as amplitudes.

This approach was tested first by simulating experimental data for the absorptionlike and dispersionlike signals as the excitation energy was varied for a set of constant applied magnetic fields; the approach of sweeping the laser energy facilitates comparison to the information on the exciton energy levels contained in Fig. 2. The microwave frequency in this case was 13.8 GHz and so the $g = 2$ spin resonance condition occurs near $B = 0.46$ T. In this simulation, the optical transition energies (which depend strongly on magnetic field) were obtained from the fits to the PLE data of Fig. 2(b). The only necessary modification of the standard three-level model for our purposes is that the optical resonance energies associated with state $|3\rangle$ are different for ingoing and outgoing photons and are $\omega_{1,3i}$ and $\omega_{2,3f}$, respectively, due to the flip-flop exchange process.[36] This process does not alter the degree of coherence in the excited intermediate state with respect to the ground state of the system.

The microwave transition energy ω_{12} was given by $\hbar\omega_{12} = g\mu_B|\mathbf{B}|$ with $g = 2$ for Mn^{2+}. The optical linewidth γ_{13} was freely adjusted, with the assumption that $\gamma_{13} = \gamma_{23}$; a value of 0.4 meV was found. The linewidth γ_{21} of the ESR transition was also fitted; this is conventionally expressed in magnetic field units and was found to be 9 mT for the experiments at 13.8 GHz and approximately the same, 7.5 mT, for those at 33.7 GHz. The occupancies of the three states were approximated as follows: $\rho_{33}^{(0)} = 0$ and $\rho_{11}^{(0)}$ was close to (but slightly greater than) $\rho_{22}^{(0)} \sim 0.5$, as is expected here since $g\mu_B|\mathbf{B}|$ and k_BT are close in magnitude. The exact ratio of $\rho_{22}^{(0)}$ to $\rho_{11}^{(0)}$ was estimated by assuming Boltzmann statistics at the helium bath temperature of 1.5 K (though the assumptions both of thermal equilibrium occupancies and of the bath temperature are not necessarily valid). The values of the γ_{ij} were assumed not to vary with magnetic field. Note also that the optical matrix elements μ_{ij} are field-independent for large-enough B and that this condition is satisfied in the current experiments.

The results of this simulation are shown in Figs. 3(a) and 3(b) for the two components of the signal [corresponding to the real and imaginary parts of S of Eq. (3)]. Here, both the experimental and calculated data were normalized to unit peak height; for clarity, we have normalized the real and imaginary parts separately but, if the same normalization

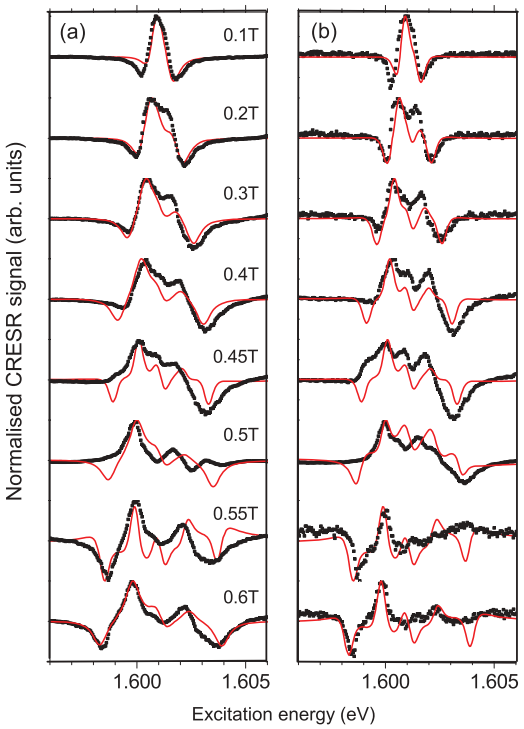

FIG. 3. (Color online) Experimental (points) and simulated (lines) coherent Raman-detected ESR signal of Mn^{2+} in unstrained (Cd,Mn)Te as a function of laser excitation energy with a microwave frequency of 13.8 GHz for the set of constant magnetic fields indicated: (a) absorptive component; (b) dispersive component. Spectra are displaced vertically for clarity.

constant were used for both components of S at a given field, the simulation also reproduces well the proportion between the two components of the experimental signal. Overall, the agreement between simulation and experiment is very good but it is worst at fields near the spin resonance condition (0.4 to 0.5 T) though the overall line shape is still reasonably well reproduced. A possible reason for the poorer agreement near exact resonance will be considered in Sec. VIII. Note that we have assumed in this simulation that the intermediate excitonic state exists in an unstrained region of the crystal; we shall consider some of the possible effects of strain in Sec. VII.

We can now proceed to consider the optically excited intermediate state. We noted in Sec. IV that this could be either the free exciton (X) or donor-bound exciton (D^0X) state.[37] The simulations of Figs. 3(a) and 3(b) resolve this question; these simulations (and all subsequent ones that we present here) only reproduce our CRESR data on the assumption of a zero-field optical transition energy of 1.6011 eV, which is not in agreement with the zero-field PLE energy (1.6038 eV) but corresponds exactly to the lower-energy SFRS resonance of Fig. 2(c). This is evident also in Fig. 4. Thus, we infer that the resonant intermediate state is, in fact, the D^0X complex and, therefore, that the optical ground state is the neutral donor D^0.

This leads to two possibilities for the source of an exchange interaction with the Mn^{2+} ions. In the lowest-energy state of the intermediate D^0X complex, the two electrons are in a spin-paired singlet state and have no exchange interaction with the Mn ions; the exciton-Mn coupling must then arise from

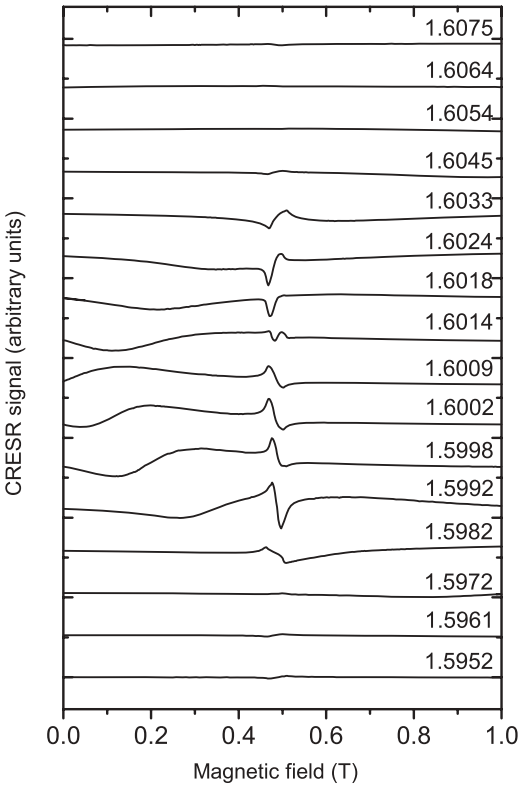

FIG. 4. Experimental coherent Raman-detected ESR signals of Mn^{2+} in (Cd,Mn)Te as a function of magnetic field with a microwave frequency of 13.7 GHz for the set of excitation laser energies indicated (in eV). Spectra are displaced vertically in equal steps for clarity; the spectra are not normalized.

the *p-d* exchange interaction between the excitonic hole and the Mn ions. Alternatively, the relevant exchange interaction could be between the Mn ions and the electron of the ground D^0 state.[37] We carried out simulations of the type discussed above for these two cases; the former predicts 12 and the latter 8 Λ-type diagrams (from the number of energetically adjacent pairs of ground spin states, multiplied by the number of possible excited spin states, multiplied by two on including Stokes and anti-Stokes processes). As a result, the CRESR signals predicted are quite different and we can only obtain the level of agreement with experiment shown in Fig. 3 on the assumption that it is the photoexcited hole of the D^0X complex that determines the coupling to the Mn ions.

It is useful to relate this to the case of (Cd,Mn)Te quantum wells, for which the SFRS spectra can show multiple Mn spin flips (of 15 or more) whose existence cannot be explained in terms of the transitions of a single Mn ion[41–43] (though the *g* factor remains identical to that of isolated Mn^{2+}). These "overtones" arise because the spins of several Mn ions within the exciton volume are polarized by their exchange interaction with the hole component of the exciton and precess about the effective magnetic field direction which is the resultant of the effective field due to the heavy hole (oriented perpendicular to the quantum well) and the externally applied field (in the plane of the quantum well).[7,41–43] The orientation of the heavy hole due to the quantum well potential, and its strong coupling to the Mn spins, are essential features of that model and also of models for the spin dynamics of two-dimensional hole gases in the presence of Mn.[44,45] In the present bulk sample, the exciton hole spin appears again to dominate the coupling to the Mn spin system, though here it is not oriented by quantum confinement effects and so the above precession mechanism does not operate; the SFRS spectra and CRESR spectra reduce once more to those of a single Mn^{2+} ion.

VI. MAGNETIC FIELD DEPENDENCE

The form of CRESR in which the magnetic field is swept (whilst keeping the excitation energy constant) yields spin-resonance spectra interpretable via standard modeling of ESR. Figure 4 (13.8 GHz) and Fig. 5 (33.7 GHz) show scans of this type over a wide magnetic field range for a set of excitation energies. In order to perform these scans over a wide field range, a relatively high microwave power was used in order to obtain a reasonable signal strength; consequently, saturation effects led to the dispersive component dominating the CRESR signal and we therefore only show data for this phase in Figs. 4 and 5. The details of the signals near the $g = 2$ resonance were presented in Sec. III and we note here only that the inversion of the $g = 2$ signal from high to low excitation energy is reproduced by the model. Partial cancellation effects between signals arising from different three-level systems mentioned in Sec. V are observed at some intermediate energies (an even clearer example of this is shown in Sec. VIII).

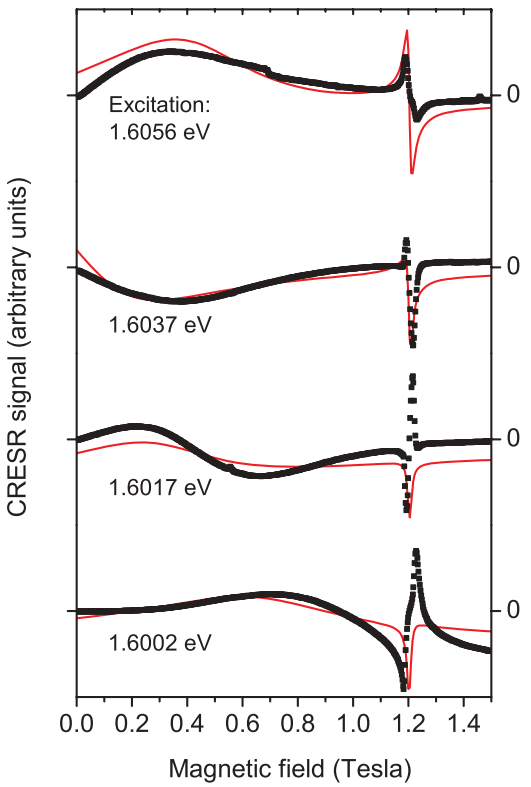

FIG. 5. (Color online) Experimental (points) and simulated (lines) coherent Raman-detected ESR signal of Mn^{2+} in (Cd,Mn)Te as a function of magnetic field with a microwave frequency of 33.7 GHz for the set of excitation laser energies indicated. Spectra are displaced vertically for clarity.

Of interest here are the comparatively broad spectral features which move in magnetic field as the optical detuning from the resonant intermediate states is altered. Such features were noted also in the CRESR spectra of Cr^{3+} in ruby; they were termed "optical resonances" to distinguish them from lines that are interpretable simply as ESR signals ("magnetic resonances"). For Cr^{3+}, the optical and magnetic resonances were expected to have the same linewidths (though they differed by up to 50% in practice);[29] here, they are clearly different, as expected because of the different mechanisms determining the respective lifetimes. Note that the relative amplitudes of the "optical" and "magnetic" resonances depend on the relative values of the parameters $\rho_{11}^{(0)}$, $\rho_{22}^{(0)}$, and $\rho_{33}^{(0)}$, so that the fits shown in Fig. 5 support our choice of those.

We show in Fig. 5 the results of applying the model discussed above (in particular, with the same excitonic energy level structure) to the swept-field data for a microwave frequency of 33.7 GHz. It is clear that it is capable of reproducing the observed behavior of the optical resonances, though the description of the line shape is not perfect; we have not included here any effects due to inhomogeneous broadening though this is, in principle, possible, for instance, by the use of a line shape which is a convolution of the fundamental, Lorentzian line with a Gaussian broadening.[19] The shape of the spin resonance signal at approximately 1.2 T is also not reproduced well here; as noted above, partial saturation of the microwave absorption led to the dominance of the dispersionlike component in the signal. This was confirmed by separate measurements in which the influence of the microwave power on the line shape was investigated over two orders of magnitude.

VII. EFFECTS DUE TO STRAIN

The PLE results of Fig. 2 demonstrate the absence of any large, homogeneous strain effects (which would produce a zero-field splitting between light- and heavy-hole transitions). This is as expected of a bulk crystal. However, we must consider the possibility that there are small, local strains in the vicinity of the exciton-Mn^{2+} system and, since the CRESR line shape is such a sensitive measure of the exciton and Mn^{2+} fine structure, we must ask what effects such strains would produce. Potentially, this is a complicated topic: Local variations in the crystal field will, in principle, modify the Mn^{2+} levels, but we disregard this effect as earlier ESR results suggest it will be small[32] (it can, however, be important in quantum wells[46]).

Here, we have focused instead on how the response of the *exciton* levels to local strains affects the CRESR results. As an example, we simulate CRESR spectra for the case of uniaxial strains oriented along the light progagation direction; the results are shown in Fig. 6. A more complete study would consider the effects of a distribution of orientations but is beyond our present scope. Our intention here is only to provide an example of how much the relative intensities of different peaks in the CRESR spectrum can vary as the sign and magnitude of the strain is changed. The spectra of Fig. 3 showed that some peaks are better reproduced by our simulations than others and, in view of the results of Fig. 6, we tentatively attribute this to the results of an experimental average over a distribution of sites with different, small strains.

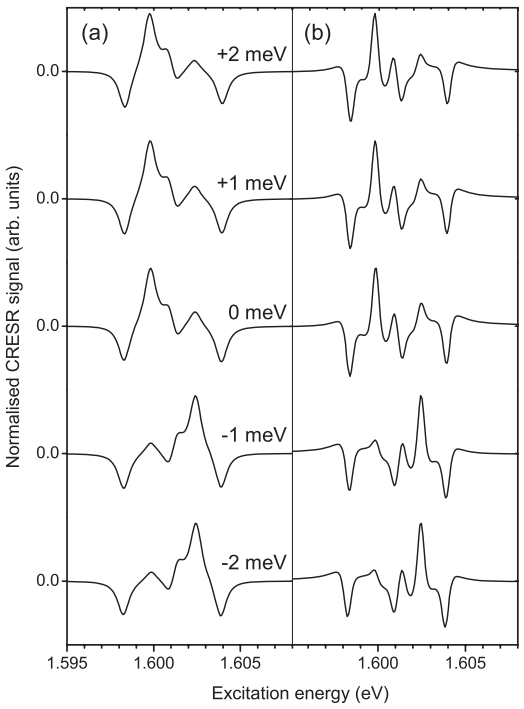

FIG. 6. Simulated CRESR signals of (Cd,Mn)Te at 13.8 GHz for a series of uniaxial strains oriented along the laser propagation direction: (left) absorptive component; (right) dispersive component.

VIII. EFFECTS DUE TO MICROWAVE HEATING

Although Fig. 5 shows one important distortion of the predicted spin resonance line shape, that due to microwave saturation, there is another, equally significant distortion which will always be of special importance in the case of DMSs. This arises because microwave-induced heating of the Mn^{2+} spin system will reduce the degree of spin polarization of the Mn^{2+} ions and will thus lead to significant shifts in the excitonic transition energies; this effect was exploited in the earliest ODMR studies of DMS.[13] Thus, the enhanced microwave absorption at the field corresponding to the $g = 2$ resonance can generate a field-dependent optical detuning even if the laser excitation is maintained nominally at the energy of an optical resonance. This effect is shown schematically in Fig. 7 and it has recently been exploited to develop a form of ODMR technique.[14,15,17,18]

Figure 8 shows experimental data focusing on the field range of the $g = 2$ magnetic resonance for low-power microwave excitation at 33.7 GHz; simulations of these data are shown in Fig. 9. First, we note that the experimental spectra show a decrease in signal strength at high excitation energies compared to the simulation. We attribute this to the decreasing intensity of the reflected beam at high photon energies; since this beam is mixed in the heterodyne detection system with the Raman-scattered light, the CRESR detection sensitivity increases with increasing intensity of the reflected beam. In principle, one could attempt to correct for the variation in reflectivity of the sample, but this is made difficult by

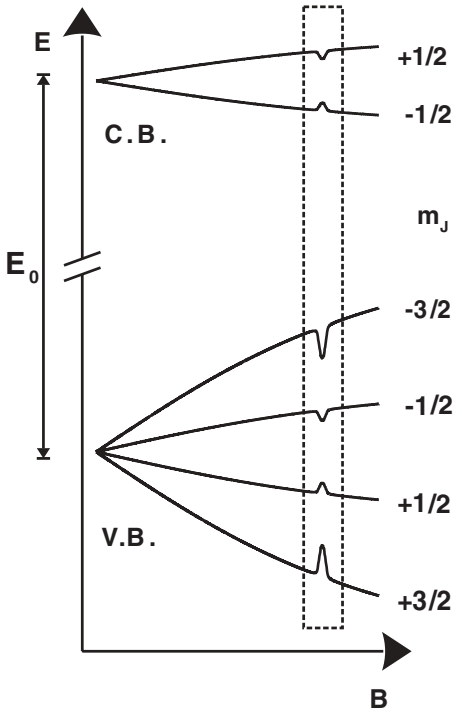

FIG. 7. Schematic diagram of the energies of conduction (CB) and valence band (VB) states of (Cd,Mn)Te as a function of magnetic field, labeled by their spin quantum numbers. The dashed box shows the region of magnetic field near the $g = 2$ spin resonance condition, where microwave heating can cause a reduction of the Mn^{2+} spin polarization.

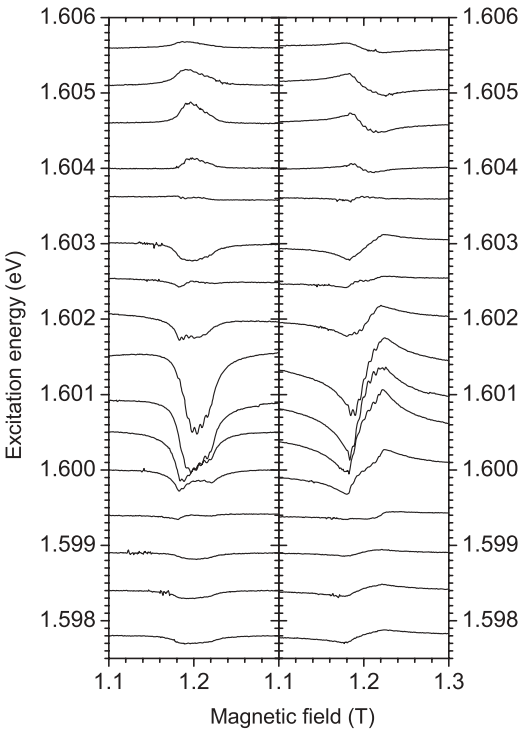

FIG. 8. Coherent Raman-detected ESR signal of Mn^{2+} in (Cd,Mn)Te at 33.7 GHz for a series of fixed excitation energies: (left) absorptive component; (right) dispersive component. A simulation of these data is shown in Fig. 9

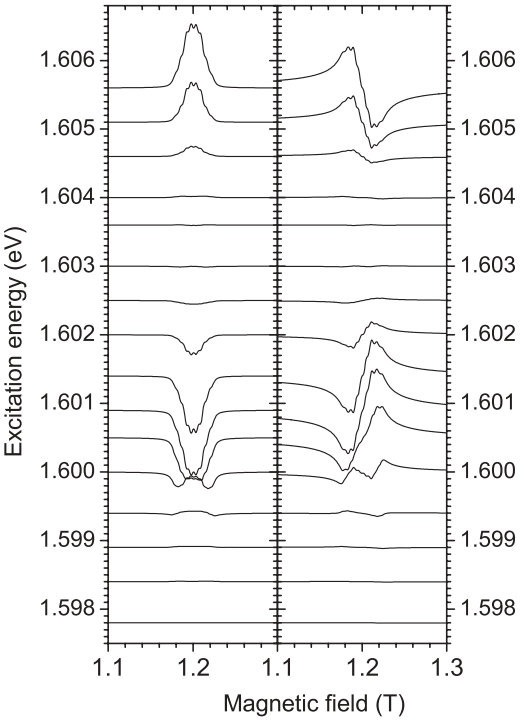

FIG. 9. Simulation of the coherent Raman-detected ESR signals of Mn^{2+} shown in Fig. 8, assuming resonance with the excitonic states of (Cd,Mn)Te and taking into account heating effects near the spin resonance condition: (left) absorptive component; (right) dispersive component.

the sensitivity of the reflectivity spectra to magnetic field, temperature and wavelength in the exciton region. For this reason, we did not attempt to make this correction (the most reliable method would be to use part of the reflected beam to provide a normalization signal measured simultaneously with the CRESR; this can be investigated in future experimental work). Finally, these spectra show a good example of cancellation of the CRESR signals at excitation energies close to the central energy of the set of exciton levels, the zero-field band gap of 1.6034 eV (Fig. 8). This cancellation is reproduced in the simulations (Fig. 9).

However, we observe one significant deviation from the expected absorption and dispersion line shapes (particularly prominent at low energies in Fig. 8) which can be attributed to the increase in temperature of the Mn^{2+} system at spin resonance. The resulting optical detuning indicated in Fig. 7 gives rise to the reduced signal strength seen, for example, in the left panel of Fig. 8 for a laser energy of 1.600 eV as a "notch" in the center of what would otherwise be a peak as seen in Fig. 1 (though in this case negative-going). To simulate this, the required magnitude of the temperature rise was about $\sim$1.0 K to 1.5 K from a base temperature of 2.5 K, very similar to that observed in the ODMR experiments.[14] It is very likely that this heating effect is also responsible for the difficulties in simulating the CRESR data near resonance that were noted in the discussion of Fig. 3. We emphasize that the temperature used in our simulations should be interpreted as the temperature of the Mn^{2+} spin system and not necessarily that of the lattice.

IX. CONCLUSIONS

We have detected electron paramagnetic resonance of Mn^{2+} ions in bulk CdTe by coherent Raman spectroscopy and we have been able to resolve the structure due to the cubic crystal field and hyperfine effects. Via a detailed description of the optical and magnetic resonances, we showed that the Mn^{2+} CRESR signal is resonant with a donor-bound exciton and arises due to the hole-Mn exchange interaction, consistent with other observations of spin-flip Raman spectroscopy of Mn^{2+} in CdTe and its heterostructures.

The detailed line shapes of the optical and magnetic resonances as functions of field and wavelength at two microwave frequencies were successfully modeled with one model and using one set of parameters for all spectra. However, resonant heating effects led to some discrepancies between data and model; the (Cd,Mn)Te system is a well-known example of a material where the optical transition energies in a magnetic field are highly sensitive to any form of heating (whether optically induced, microwave-induced, or otherwise) due to the Brillouin function dependence of the band states on field and temperature.

Finally, our results demonstrate that the coherence between optical (excitonic) and spin (Mn) excitations is maintained even in case where the intermediate state for Raman scattering couples to the paramagnetic center only via an exchange interaction. In this case, the relevant exchange was shown to be the $p-d$ exchange interaction between the hole of the donor-bound exciton and the Mn ions. This result has the important consequence of demonstrating that the use of the CRESR technique for the optical detection of ESR is not limited only to systems where the optical transitions take place between the electronic states of the paramagnetic center itself. Our results show that the complex formed by the donor-bound exciton and the Mn^{2+} ions within its radius can be adequately described by a three-level model such as discussed in the context of donor-bound electrons in the absence of Mn^{2+}[8].

ACKNOWLEDGMENTS

This work was supported by the EPSRC (UK) under Grant No. GR/R38231/01 and INTAS 03-51-5266.

[1] T. Dietl, Nat. Mater. **9**, 965 (2010).
[2] B. Jusserand, F. Perez, D. R. Richards, G. Karczewski, T. Wojtowicz, C. Testelin, D. Wolverson, and J. J. Davies, Phys. Rev. Lett. **91**, 086802 (2003).
[3] F. Perez, C. Aku-leh, D. Richards, B. Jusserand, L. C. Smith, D. Wolverson, and G. Karczewski, Phys. Rev. Lett. **99**, 026403 (2007).
[4] A. Haury, A. Wasiela, A. Arnoult, J. Cibert, S. Tatarenko, T. Dietl, and Y. M. d'Aubigné, Phys. Rev. Lett. **79**, 511 (1997).
[5] A. Winter, H. Pascher, H. Krenn, I. Miotkowski, and A. K. Ramdas, Phys. Rev. B **78**, 045213 (2008).
[6] C. Le Gall, L. Besombes, H. Boukari, R. Kolodka, J. Cibert, and H. Mariette, Phys. Rev. Lett. **102**, 127402 (2009).
[7] J. M. Bao, A. V. Bragas, J. K. Furdyna, and R. Merlin, Phys. Rev. B **71**, 045314 (2005).
[8] K.-M. C. Fu, S. M. Clark, C. Santori, C. R. Stanley, M. C. Holland, and Y. Yamamoto, Nat. Phys. **4**, 780 (2008).
[9] L. C. Smith, S. J. Bingham, J. J. Davies, and D. Wolverson, Appl. Phys. Lett. **87**, 202101 (2005).
[10] L. C. Smith, D. Wolverson, S. J. Bingham, and J. J. Davies, Phys. Status Solidi B **243**, 892 (2006).
[11] D. L. Peterson, D. U. Bartholomew, U. Debska, A. K. Ramdas, and S. Rodriguez, Phys. Rev. B **32**, 323 (1985).
[12] A. Abragam and B. Bleaney, *Electron Paramagnetic Resonance of Transition Metal Ions* (Oxford University Press, Oxford, 1970).
[13] A. V. Komarov, S. M. Ryabchenko, O. V. Terletskii, I. I. Zheru, and R. D. Ivanchuk, Zh. Eksp. Teor. Fiz.**73**, 608 (1977) [Sov. Phys. JETP **46**(2), 318 (1977)].
[14] M. Sadowski, M. Byszewski, and M. Potemski, Appl. Phys. Lett. **82**, 3719 (2003).
[15] M. Byszewski, D. Plantier, M. L. Sadowski, M. Potemski, A. Sachrajda, Z. Wilamowski, and G. Karczewski, Phys. E (Amsterdam, Neth.) **22**, 652 (2004).
[16] S. Zeng, L. C. Smith, J. J. Davies, D. Wolverson, S. J. Bingham, and G. N. Aliev, Phys. Status Solidi B **243**, 887 (2006).
[17] V. Y. Ivanov, M. Godlewski, D. R. Yakovlev, S. M. Ryabchenko, G. Karczewski, and A. Waag, Phys. Status Solidi A **204**, 174 (2007).
[18] V. Y. Ivanov, M. Godlewski, D. R. Yakovlev, M. K. Kneip, M. Bayer, S. M. Ryabchenko, and A. Waag, Phys. Rev. B **78**, 085322 (2008).
[19] K. Holliday, X. F. He, P. T. H. Fisk, and N. B. Manson, Opt. Lett. **15**, 983 (1990).
[20] N. B. Manson, J. P. Harrison, and M. J. Sellars, Phys. Rev. B **74**, 104303 (2006).
[21] B. Borger, J. Gutschank, D. Suter, A. J. Thomson, and S. J. Bingham, J. Am. Chem. Soc. **123**, 2334 (2001).
[22] S. J. Bingham, T. Rasmussen, J. Farrar, D. Wolverson, and A. J. Thomson, Mol. Phys. **105**, 2169 (2007).
[23] S. J. Bingham, D. Wolverson, and A. J. Thomson, Biochemical Soc. Trans. **36**, 1187 (2008).
[24] M. P. Halsall, D. Wolverson, J. J. Davies, D. E. Ashenford, and B. Lunn, Solid State Commun. **86**, 15 (1993).
[25] C. Orange, B. Schlichtherle, D. Wolverson, J. J. Davies, T. Ruf, K. I. Ogata, and S. Fujita, Phys. Rev. B **55**, 1607 (1997).
[26] S. J. Bingham, J. J. Davies, and D. Wolverson, Phys. Rev. B **65**, 155301 (2002).
[27] J. Mlynek, N. C. Wong, R. G. DeVoe, E. S. Kintzer, and R. G. Brewer, Phys. Rev. Lett. **50**, 993 (1983).
[28] N. C. Wong, E. S. Kintzer, J. Mlynek, R. G. DeVoe, and R. G. Brewer, Phys. Rev. B **28**, 4993 (1983).
[29] M. O. Schweika-Kresimon, J. Gutschank, and D. Suter, Phys. Rev. A **66**, 043816 (2002).
[30] S. Tsoi, I. Miotkowski, S. Rodriguez, A. K. Ramdas, H. Alawadhi, and T. M. Pekarek, Phys. Rev. B **69**, 035209 (2004).
[31] J. K. Furdyna, J. Appl. Phys. **64**, R29 (1988).
[32] J. Lambe and C. Kikuchi, Phys. Rev. **114**, 1256 (1960).

[33]S. J. Bingham, D. Suter, A. Schweiger, and A. J. Thomson, Chem. Phys. Lett. **266**, 543 (1997).
[34]M. Hirsch, R. Meyer, and A. Waag, Phys. Rev. B **48**, 5217 (1993).
[35]A. Petrou, D. L. Peterson, S. Venugopalan, R. R. Galazka, A. K. Ramdas, and S. Rodriguez, Phys. Rev. B **27**, 3471 (1983).
[36]J. Stühler, M. Hirsch, G. Schaack, and A. Waag, Phys. Rev. B **49**, 7345 (1994).
[37]S. M. Ryabchenko and Y. G. Semenov, Phys. Status Solidi B **134**, 281 (1986).
[38]N. Bloembergen, Phys. Rev. **120**, 2014 (1960).
[39]M. Mitsunaga, E. S. Kintzer, and R. G. Brewer, Phys. Rev. B **31**, 6947 (1985).
[40]T. Blasberg and D. Suter, Phys. Rev. B **51**, 12439 (1995).
[41]J. Stühler, G. Schaack, M. Dahl, A. Waag, G. Landwehr, K. V. Kavokin, and I. A. Merkulov, Phys. Rev. Lett. **74**, 2567 (1995).
[42]J. Stühler, G. Schaack, M. Dahl, A. Waag, G. Landwehr, K. V. Kavokin, and I. A. Merkulov, Phys. Rev. Lett. **74**, 4966 (1995).
[43]L. C. Smith, J. J. Davies, D. Wolverson, M. Lentze, J. Geurts, T. Wojtowicz, and G. Karczewski, Phys. Rev. B **77**, 115341 (2008).
[44]K. V. Kavokin and I. A. Merkulov, Phys. Rev. B **55**, R7371 (1997).
[45]K. V. Kavokin, Phys. Rev. B **59**, 9822 (1999).
[46]J. K. Furdyna, M. Qazzaz, G. Yang, L. Montes, S. H. Xin, and H. Luo, Acta Phys. Pol. A **88**, 607 (1995).